AGU PUBLICATIONS

JGR

Journal of Geophysical Research: Oceans

RESEARCH ARTICLE

10.1002/2014JC009866

Special Section:
Pacific-Asian Marginal Seas

Summertime Changjiang River plume variation during 1998–2010

Yan Bai[1,2], Xianqiang He[1], Delu Pan[1,2], Chen-Tung Arthur Chen[1,3], Yan Kang[4], Xiaoyan Chen[1], and Wei-Jun Cai[5]

[1]State Key Laboratory of Satellite Ocean Environment Dynamics, Second Institute of Oceanography, State Oceanic Administration, Hangzhou, China, [2]Institute of Remote Sensing and Earth Science, Hangzhou Normal University, Hangzhou, China, [3]Institute of Marine Geology and Chemistry, National Sun Yat-sen University, Kaohsiung, Taiwan, [4]Institute of Economic and Social Development, Zhejiang University of Finance and Economics, Hangzhou, China, [5]School of Marine Science and Policy, University of Delaware, Newark, Delaware, USA

Abstract Using an improved satellite-derived salinity algorithm in the East China Sea (ECS), we presented and examined a general view on summertime Changjiang River plume variation during 1998–2010. Three types of plume shapes were identified: (1) the commonly known northeastward transportation, (2) a case in which most of the plume water crossed the Cheju Strait into the Tsushima-Korea Straits with only a small fraction staying on the shelf of the ECS, and (3) a rare case in which the plume front moved southeastward. Satellite time-series data suggested that, during the peak river discharge time in July with favorable southwest monsoon, the plume area was highly correlated with the river discharge of the same month. Interestingly, the plume area in August was also dominated by the discharge in July. In August, as the direct effect of freshwater discharge weakening, the plume area also became positively correlated with wind speed in the 45° and 60°direction, suggesting that the plume extension was more influenced by the southwesterly wind during periods of smaller discharge. Furthermore, a few special cases with unique plume extensions were found under extreme weather conditions. Finally, we found no significant long-term trend of plume area change over 1998–2010 in summertime and concluded that the interannual variation was probably regulated by natural variation rather than anthropogenic effects, such as construction of the Three Gorges Dam. This study will have implications for biogeochemical and modeling studies in large river plume areas.

Key Points:
- Summertime Changjiang River plumes were highly variable during 1998–2010
- Besides the well-known plume pattern, two additional types were identified
- Relationships between plume areas and discharge were quantitatively clarified

Correspondence to:
Y. Bai,
baiyan_ocean@126.com

Citation:
Bai, Y., X. He, D. Pan, C.-T. A. Chen, Y. Kang, X. Chen, and W.-J. Cai (2014), Summertime Changjiang River plume variation during 1998–2010, *J. Geophys. Res. Oceans*, *119*, 6238–6257, doi:10.1002/2014JC009866.

Received 29 JAN 2014
Accepted 21 AUG 2014
Accepted article online 26 AUG 2014
Published online 17 SEP 2014

1. Introduction

Approximately 40% of the freshwater and particulate material transported into the oceans comes from the world's 10 largest rivers [*Dagg et al*., 2004]. Understanding the variation of large river plume systems is crucial to studies of material transport and biogeochemical processes in marginal seas. The Changjiang (Yangtze) River, the largest in the Eurasian continent and the fifth largest river in the world in terms of volume discharge, flows into the East China Sea (ECS), one of the most productive marginal seas [*Su*, 1998; *Liu et al*., 2003; *Chen*, 2009]. The Changjiang River discharge accounts for ~90% of the total river discharge into the Yellow Sea and the ECS, and the annual average freshwater influx from rainfall is nearly balanced by evaporation from the ECS [*Chen et al*., 1994]. Thus, any variation in the Changjiang River discharge and its carrying materials could have significant implications for the ECS and even the adjacent Japan Sea [*Chen et al*., 1994; *Siswanto et al*., 2008].

In the past two decades, marked changes in the Changjiang River discharge has occurred several times. For example, 1998 and 2010 were extreme flood years. In addition, the first filling stage of the world's largest dam, the Three Gorges Dam, was completed in June 2003, and full-scale operations began in 2009. The year 2006 was the worst drought year in the past 50 years, coinciding with an increase of water level in the Three Gorges Dam from 135 to 156 m [*Dai et al*., 2008; *Chu et al*., 2009]. In some studies based on field data, the area of the Changjiang River Plume on the shelf of the ECS has been related to the Changjiang River discharge [e.g., *Chen et al*., 2009; *Tseng et al*., 2011]. In other studies, researchers have further speculated that the Three Gorges Dam has influenced the air–sea carbon flux [*Chen et al*., 2008b; *Tseng et al*., 2011], primary production [*Gong et al*., 2006], and microbial community structure [*Jiao et al*., 2007] in the ECS. However, owing to the lack of time-series data, the effects of the discharge on the plume area and corresponding

biogeoscience processes cannot be identified clearly. Moreover, studies based on limited field surveys are inefficient for demonstrating clearly the effect of human activities and natural changes over long time scales.

Although it has been recognized that defining plume areas from satellite images is a useful method, the relevant research is still sparse in the ECS. *Kim et al*. [2009] related chlorophyll *a* concentration to salinity in the Changjiang plume area and presented the monthly summer plume area within a limited area during 1998–2007. A more reasonable approach to retrieve satellite-derived salinity is based on the conservative behavior of the absorption coefficient of colored dissolved organic matter (a_{CDOM}) [*Sasaki et al*., 2008; *Ahn et al*., 2008; *Bai et al*., 2013]. The new orbiting microwave sensor of the Soil Moisture and Ocean Salinity (SMOS) (launched on November 2009) and Aquarius/SAC-D (launched on June 2011) are specially designed for measuring the global salinity field, but they have shorter time-series data and a coarser spatial scale (∼30–100 km) compared with the ocean color data. Thus, until now, there are still no time-series data of the Changjiang River plume areas that can reveal its interannual variation or aid in evaluating the quantitative relationship between the discharge and the plume area.

Based on *Bai et al*.'s [2013] satellite-derived salinity algorithm in the ECS, we present a synthetic view of the spatial-temporal variation of the Changjiang River plume in July and August (the months of largest river discharge) during 1998–2010. We first present the data and method in section 2. Then, in section 3, we improve and validate the satellite-derived salinity algorithm with in situ data to ensure a credible satellite salinity data set for further analysis. In section 4, we show the interannual variation of plume area, identify the plume shapes during the summer, and clarify the relationship between the plume area and the discharge. In section 5, we discuss the possible influence of river discharge and wind on the plume distribution. Finally, we derive our conclusions and discuss the implications of the variation of the Changjiang River plume on the biogeochemistry of the region.

2. Data and Method

2.1. Research Area

The ECS has broad shelf areas with a width of around 500 km (0–200 m isobaths). It extends from Cheju Island in the north to Taiwan Island in the south, and it is bordered by the Kuroshio on the east and the coast of China on the west. The circulation and biogeochemical features of the ECS have been well documented in the literature [e.g., *Su*, 1998; *Chang and Isobe*, 2003; *Liu et al*., 2003; *Chen*, 2009, etc.]. The strong western ocean boundary current Kuroshio flows northeastward along the shelf break of the ECS. The intrusion of the Kuroshio off northeastern Taiwan Island combined with the northward flow from the Taiwan Strait forms the northward Taiwan Warm Current in summer. The Changjiang River plume (also known as the Changjiang Diluted Water) extends to the northeast toward the Tsushima-Korea Straits during summer. In this paper, we focus on the extension of the Changjiang plume in summer within the area of 26°–36°N and 118°–132°E, which includes the southern Yellow Sea, the shelf of the ECS, and the Tsushima-Korea Straits (Figure 1).

2.2. Satellite Data

The daily remote sensing reflectance (Rrs) and chlorophyll *a* concentration (chla) retrieved by the Sea-viewing Wide Field-of-view Sensor (SeaWiFS) in July and August 1998–2010 were acquired from the ocean color website (http://oceancolor.gsfc.nasa.gov) of the U.S. National Aeronautics and Space Administration (NASA) for the retrieval of surface water salinity. These were level 3 products (L3) with a spatial resolution of ∼9 km. The available SeaWiFS data came from September 1997 to December 2010, but data were unavailable for July 2008 owing to sensor failure. To achieve consistent time-series data, we only used the SeaWiFS data, though there are data from other ocean color sensors, such as the Moderate-resolution Imaging Spectro-radiometer (MODIS). In addition, for validation of the satellite-derived salinity, we also downloaded the level 2 (L2) remote sensing reflectance (Rrs) data with native resolution (∼1 km), corresponding to the in situ data period.

In addition, we used the cross-calibrated multiplatform (CCMP) ocean surface wind data to analyze the wind field variation in the ECS. The CCMP data set provided by the Physical Oceanography Distributed Active Archive Centre (PO.DAAC, http:/podaac.jpl.nasa.gov) has a spatial resolution of 0.25°. The data were

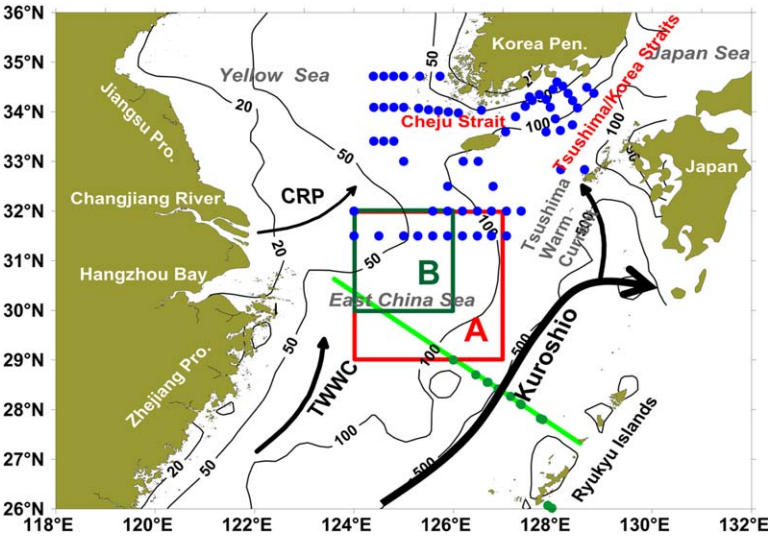

Figure 1. Research region and matching stations for the in situ salinity and daily SeaWiFS-derived salinity data during 1998–2010. The data in blue and green dots were downloaded from KODC and JMA, respectively. The straight green line is the PN section. Arrows denote schematic summer surface currents in the East China Sea [*Yuan et al*., 2008]. CRP: Changjiang River plume; TWWC: Taiwan Warm Current; the Tsushima Warm Current is also known as the Kuroshio Branch Current. The squares in red and dark green are the domain used to calculate the wind speed in Figure 8.

derived through the cross calibration and assimilation of data from several sensors with SSM/I, TMI, AMSR-E, SeaWinds on QuikSCAT, and SeaWinds on ADEOS-II, which were also combined with conventional observations and a starting estimate of the wind field using a variational analysis method. The data sets cover the whole global ocean for the period beginning in 1987, making them extremely useful for atmospheric and oceanic research and for air–sea interaction studies [*Atlas et al*., 2008, 2011].

2.3. In Situ Data

Surface salinity data were obtained from the U.S. National Oceanographic Data Center (NODC). Data originating from the Korea Oceanographic Data Center (KODC) are available up to 2005, with salinity data regularly acquired in February, April, June, August, October, and December in each year. We also downloaded surface salinity data in serial oceanographic survey data sets from the Japan Meteorological Agency (JMA).

Changjiang River discharge data were downloaded from the website of the Ministry of Water Resources of the People's Republic of China (http://www.hydroinfo.gov.cn). The discharges were measured at the hydrological gauge station, Datong, which suffers from no tidal influence and is 624 km upstream from the river mouth.

Typhoon records were downloaded from the Joint Typhoon Warning Center (JTWC; http://weather.unisys.com/hurricane/w_pacific). The data include typhoon center position in latitude and longitude, time (UTC), maximum sustained winds (in knots), and typhoon scale every 6 h. We only selected typhoons (including subtropic storms) occurring during July and August and entering the area of 24°–40°N and 118°–135°N, where the wind circle might affect the plume extension.

To relate the long-term changes in plume variation with the El Niño–Southern Oscillation (ENSO) and Pacific Decadal Oscillation (PDO), we downloaded the Multivariate ENSO Index (MEI) and PDO index from the websites http://www.esrl.noaa.gov/psd/enso/mei/ and http://jisao.washington.edu/pdo/, respectively.

2.4. Calculation of Plume Area

In this paper, we focus on the monthly variation of plume area. The monthly composite salinity was combined from the daily satellite-derived salinity. We calculated the plume area within four salinity thresholds (28, 29, 30, and 31) for comparison. First, contour maps of the monthly satellite-derived salinity were drawn with Surfer software, then files of individual salinity isohalines were input into ArcGIS software for the area calculation. As the Changjiang River plume extends offshore, a main isohaline exists for every individual isohaline (28, 29, 30, and 31), and the area enclosed by each main isohaline and the coastal line of mainland China was calculated within the region shown in Figure 1 (26°–36°N, 119°–132°E). The other small isohaline

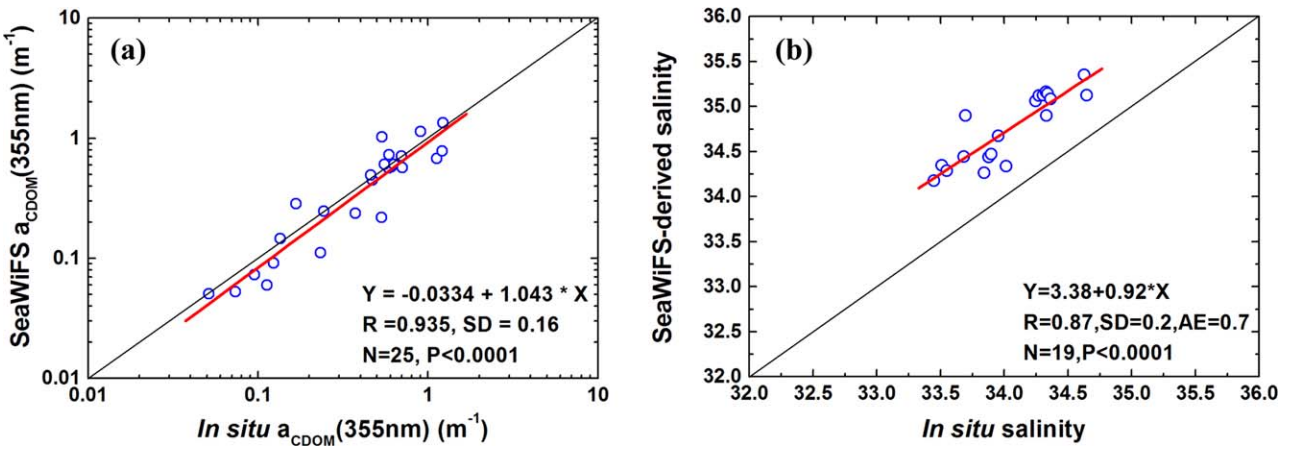

Figure 2. (a) Comparison of the daily satellite-derived $a_{CDOM}(355)$ and the in situ $a_{CDOM}(355)$. (b) Comparison of the daily satellite-derived salinity and the in situ salinity from JMA. Spatial resolution of satellite data is ~9 km.

circles inside and outside the main isohaline were not included in the area calculation, because our focus was on the general plume distribution on a monthly scale. Near-shore areas within 50 m isobaths around the Korean Peninsula and the coast around Japan were also excluded in the plume area calculation.

3. Satellite-Derived Salinity Algorithm and Validation

3.1. Improvement of Satellite Salinity Algorithm

Bai et al. [2013] have established the following linear relationship between the absorption coefficient of colored dissolved organic matter at 355 nm ($a_{CDOM}(355)$) and sea surface salinity (SSS) based on seasonal data with a full salinity range and wide coverage of the Changjiang River–dominated ECS:

$$\mathrm{SSS} = 35.595 - 14.151 \times a_{CDOM}(355) \quad (1)$$

With the satellite-derived a_{CDOM}, the surface salinity can be mapped in the ECS. In addition, *Bai et al.* [2013] pointed out that there were two major factors that would affect the accuracy of the satellite-derived salinity data: 1) the accuracy of satellite-derived a_{CDOM} and 2) the seasonal change in the marine end-member salinity. In this study, we further checked these two issues, adding more abundant in situ data and improving the algorithm.

Bai et al. [2013] have validated and compared three published a_{CDOM} algorithms and found that algorithm of *Carder et al.* [2003] had the best performance in the ECS. Through the estimation of spectral slope (S_{CDOM}), $a_{CDOM}(355)$ could be retrieved from $a_{CDOM}(412)$ and $a_{CDOM}(443)$ based on *Carder et al.*'s [2003] a_{CDOM} algorithm. The detailed explanation of the algorithm can be found in *Bai et al.* [2013]. In turbid coastal waters, the accuracy of the satellite-derived a_{CDOM} would be influenced by the standard atmospheric correction algorithm based on the near-infrared wavelength, as well as by terrestrial particles and dissolved organic matter [*Zhu et al.*, 2011; *He et al.*, 2012; *Bai et al.*, 2013]; however, these are not importance issues for summertime river plumes, in which water is stratified with fewer suspended particles in the shelf of the ECS.

Based on the $a_{CDOM}(355)$ algorithm from *Bai et al.* [2013], we generated the daily satellite-derived $a_{CDOM}(355)$ for July and August over 1998–2010 (marked as $a_{CDOM}(355)_{@1}$), and then matched the $a_{CDOM}(355)_{@1}$ with the in situ $a_{CDOM}(355)$ data from eight cruises in the ECS (for detailed information, see *Bai et al.* [2013]). As shown in Figure 2a, $a_{CDOM}(355)_{@1}$ agreed with the in situ data well, although it was slightly and systematically underestimated. To obtain more accurate results, we used a corrected equation for the satellite-derived $a_{CDOM}(355)_{@1}$ (marked as $a_{CDOM}(355)_{@2}$):

$$a_{CDOM}(355)_{@2} = -0.0334 + 1.043 \times a_{CDOM}(355)_{@1} \quad (2)$$

Thus this $a_{CDOM}(355)_{@2}$ is used instead of the $a_{CDOM}(355)$ in equation (1).

Equation (1) was based on conservative mixing between freshwater and marine end-members, a relationship established from in situ data from all seasons to ensure large enough statistical samples. For the marine end-member, the salinity in the outer boundary of the shelf (Kuroshio) also exhibits small seasonal changes

(e.g., it was ~33.2–34 in summer and ~34.5 in winter) [*Bai et al*., 2013]. The lower marine end-member salinity in summer was probably the combined result of a greater river discharge during summer and a seasonal variation in the position of the Kuroshio Current, making the surface layer salinity in the outer shelf a little bit lower in summer (Kuroshio outward) than in winter (Kuroshio shelfward) [*Chen*, 2008; *Liu and Gan*, 2012]. Therefore, a proper correction method should be established to adjust for this variation.

Because the KODC data did not cover the Kuroshio, we used the JMA data to correct the bias of the satellite-derived marine end-member salinity. We matched the daily satellite-derived salinity after correcting equation (2) in July and August with the in situ surface salinity data during 1998–2010 from JMA. Owing to heavy cloud coverage and the limited availability of daytime-measured in situ data, we only matched up data at a few most frequently measured stations along the PN section in the outer shelf (Figure 1). The satellite-derived salinity correlates well with the in situ data but systematically overestimates the data (Figure 2b). We thus corrected the derived SSS using

$$\mathrm{SSS(summer)} = \mathrm{SSS} - 0.7 \tag{3}$$

The offset of 0.7 is the average bias of 19 JMA matchup points for the high-salinity end-member ranging from 33.2 to 34.5. Because of the linear relationship between salinity and $a_{CDOM}(355)$ (equation (1)), the magnitude of the correction owing to the overestimation of the marine end-member should linearly decrease as the salinity decreases. However, the variation of the correction is negligible (<0.2) for salinity > 28. Therefore, we adopted a fixed correction for the high salinity range. In summary, the final satellite-derived salinity data that we used were based on equation (1) [*Bai et al*., 2013], combined with the two correction terms given in equations (2) and (3).

3.2. Validation of the Satellite-Derived Salinity Data

We generated the satellite-derived salinity data in the summertime ECS. We used a totally independent in situ salinity data set from KODC (1998–2005) to validate the daily satellite-derived salinity data. We followed the validation method proposed by *Bailey and Werdell* [2006] using the level 2 data of SeaWiFS with a spatial resolution of ~1 km. To obtain more valid matchups, we used a time window of ±24 h instead of the ±3 h used by *Bailey and Werdell* [2006]. Because of the regular measurement in time series of the KODC data, we were able to gain 108 matched data points (see Figure 3). In general, the majority of the matchup data fit the 1:1 line well with an absolute error of ±1.0 salinity units (Figure 3a), demonstrating that the satellite-derived salinity data are reliable. Based on the corrected algorithms, we also updated our early comparison between satellite-derived salinity and in situ underway measurements during 16–31 August 2009 in *Bai et al*. [2013] (Figure 3c). The performance of the salinity algorithms exhibited significant improvement, especially for the high salinities in the outer shelf and Kuroshio, which demonstrated the efficacy of using the offset correction for the marine end-member of salinity in summer.

It needs to be noted that there are spatial and temporal gaps between field-measured salinity (taken instantaneously at one point) and daily satellite-derived salinity (taken around noon and averaged in 9×9 km areas). These gaps may be more significant for the highly dynamic plume areas, which could also contribute to the seemingly large overall uncertainty of ±1.0 salinity units. Most of the significantly underestimated satellite data were located in the turbid waters around the Korean Peninsula under the influence of terrestrial inputs, which differ from the source from the Changjiang River (Figure 3b). Other points with large bias in the shelf would be affected by the autochthonous biological effect of large blooms (resulting in an underestimate) or bacterial consumption (resulting in an overestimate). However, the patchiness of these biological effects may not affect the plume identification from space on a large scale, as pointed out in *Bai et al*. [2013].

In this paper, we focus on the monthly scale of plume extension, so we also compared the monthly satellite results with the monthly contour maps derived from the in situ salinity data in August from the KODC data set (Figure 4). In general, the satellite maps captured similar structural details of the plume area, such as the relatively high salinity (~31–32) water mass in the middle of the Yellow Sea and the various extensions in different years to Cheju Island and the Tsushima-Korea Straits. The difference between satellite-derived salinity and the in situ salinity field should be mainly caused by their different time scales. The satellite-derived salinity values are the monthly averaged values from the daily salinity field with synchronous observation, whereas the in situ salinity is an instantaneous value at a station. In this sense, the satellite-derived plume distribution is more reasonable than the contour maps derived from the field survey that covers a certain period.

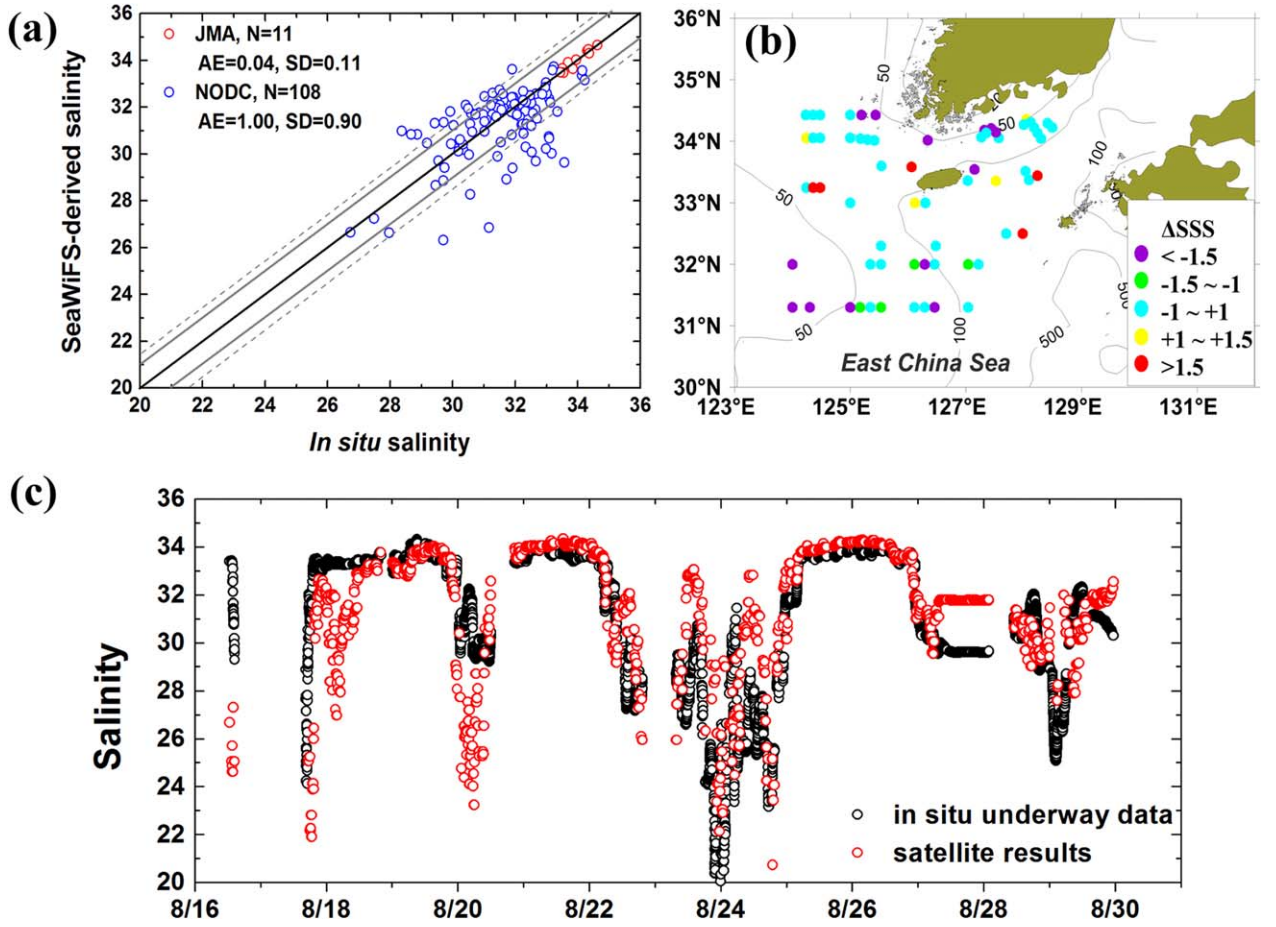

Figure 3. (a) Comparison of the corrected satellite-derived salinity (a spatial resolution of ~1 km) and the in situ salinity from KODC (blue dots) and JMA (red dots). The black line is the 1:1 line. The solid gray lines mark an absolute salinity error of ±1 and the dotted gray lines mark an absolute salinity error of ±1.5. (b) Locations of the absolute error (AE) between the satellite-derived salinity and the in situ salinity (marked ΔSSS). (c) Point-to-point comparison between the satellite-derived salinity and the in situ data from underway measurements during 16–31 August 2009, which updates the results from *Bai et al.* [2013] based on the improved algorithms. Note that the time windows of the underway measurement and satellite data were 1 min and a 16 day averages, respectively.

With the salinity used as a threshold, we cannot distinguish the Changjiang River plume with residual Changjiang diluted water in previous years in the Yellow Sea. However, salinities in the middle basin of the Yellow Sea were always >32 in winter (February), as determined from the climatology distributions of surface layer salinity [*Chen et al.*, 2009]. Thus, we believe the influence of residual Changjiang diluted water in the previous years in the Yellow Sea is limited to the summertime plume. Meanwhile, the influence of other runoff and precipitation in the southern Yellow Sea can be neglected compared to the influence of the huge Changjiang River discharge in summer [*Chen et al.*, 2009].

Some low-salinity patches within the plume were also found in the monthly maps (Figure 4). These may be the result of 1) the composite results from the daily satellite-derived salinity maps or the discrete field measurements in one month and/or 2) patches of low-salinity water extending eastward, rather than spreading as a tongue-shaped pattern from the Changjiang [*Lie et al.*, 2003; *Chen et al.*, 2008a]. This is a very interesting phenomenon and worth further study with daily satellite imagery under clear weather. However, in this study, we focused only on the monthly scale.

4. Variation of the Changjiang River Plume

4.1. Extending Shapes of the Changjiang River Plume

The satellite-derived monthly Changjiang River plumes in July and August during 1998–2010 are shown in Figure 5. The plume is directed generally northeastward, entering the Tsushima-Korea Straits and Japan

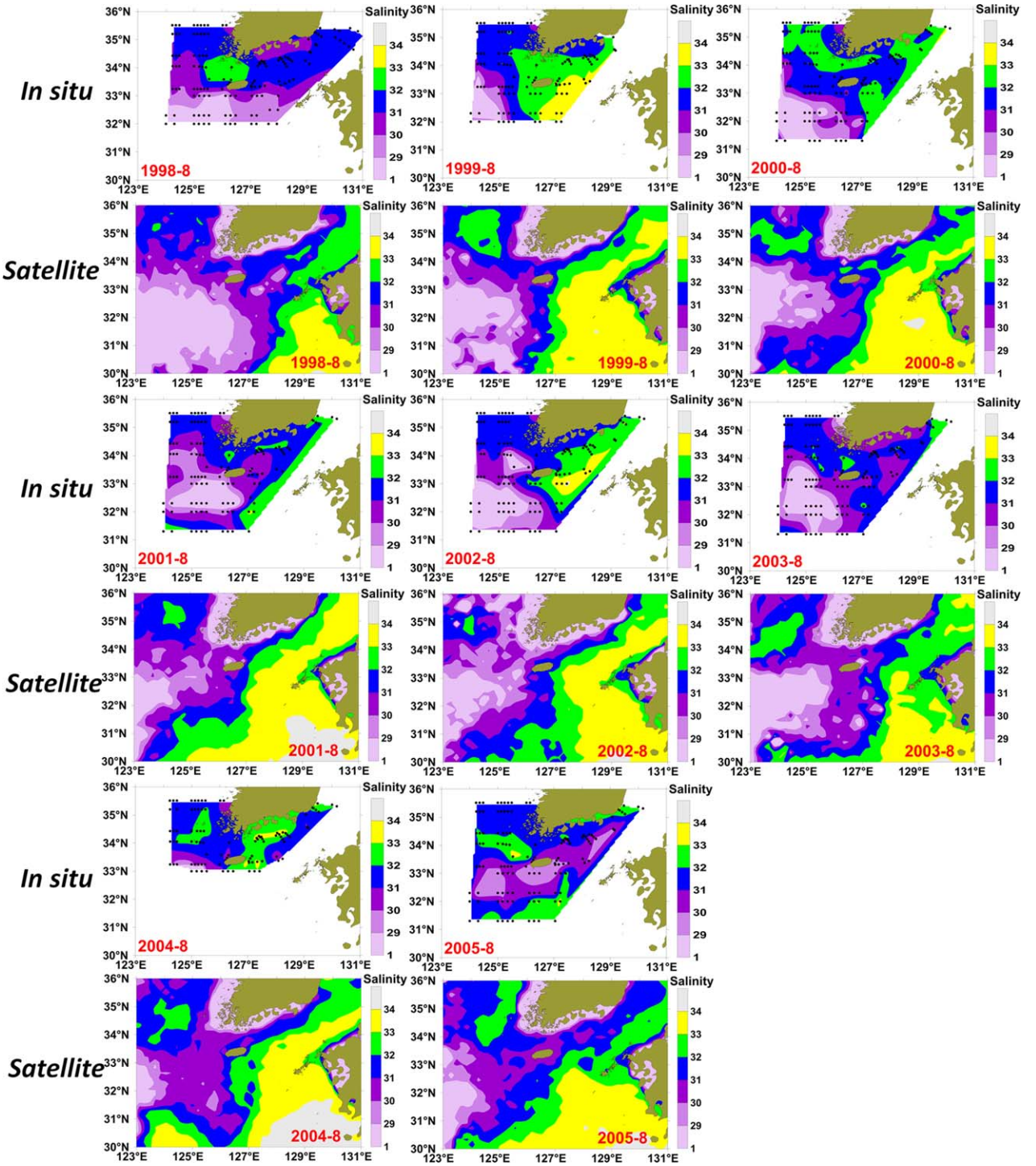

Figure 4. Comparison between monthly salinity distributions from the field-measured KODC data in August and monthly satellite-derived salinity on the same color scale.

Sea. The isohalines are nearly parallel with the isobaths, especially the <50 m isobaths with less saline water. Low-salinity water widely occupies the coastal area of Jiangsu province (north of the Changjiang Estuary) and is restricted to the coastal area of Zhejiang province (south of the Changjiang Estuary).

Based on the 31 isohaline, three major types of extending shapes of the Changjiang River plume could be identified (Figures 5 and 6). Type 1 comprises plumes extending northeastward. This type is similar to the common climatologic plume shape in summer [e.g., *Chen*, 2008]. The plumes cross the Tsushima-Korea

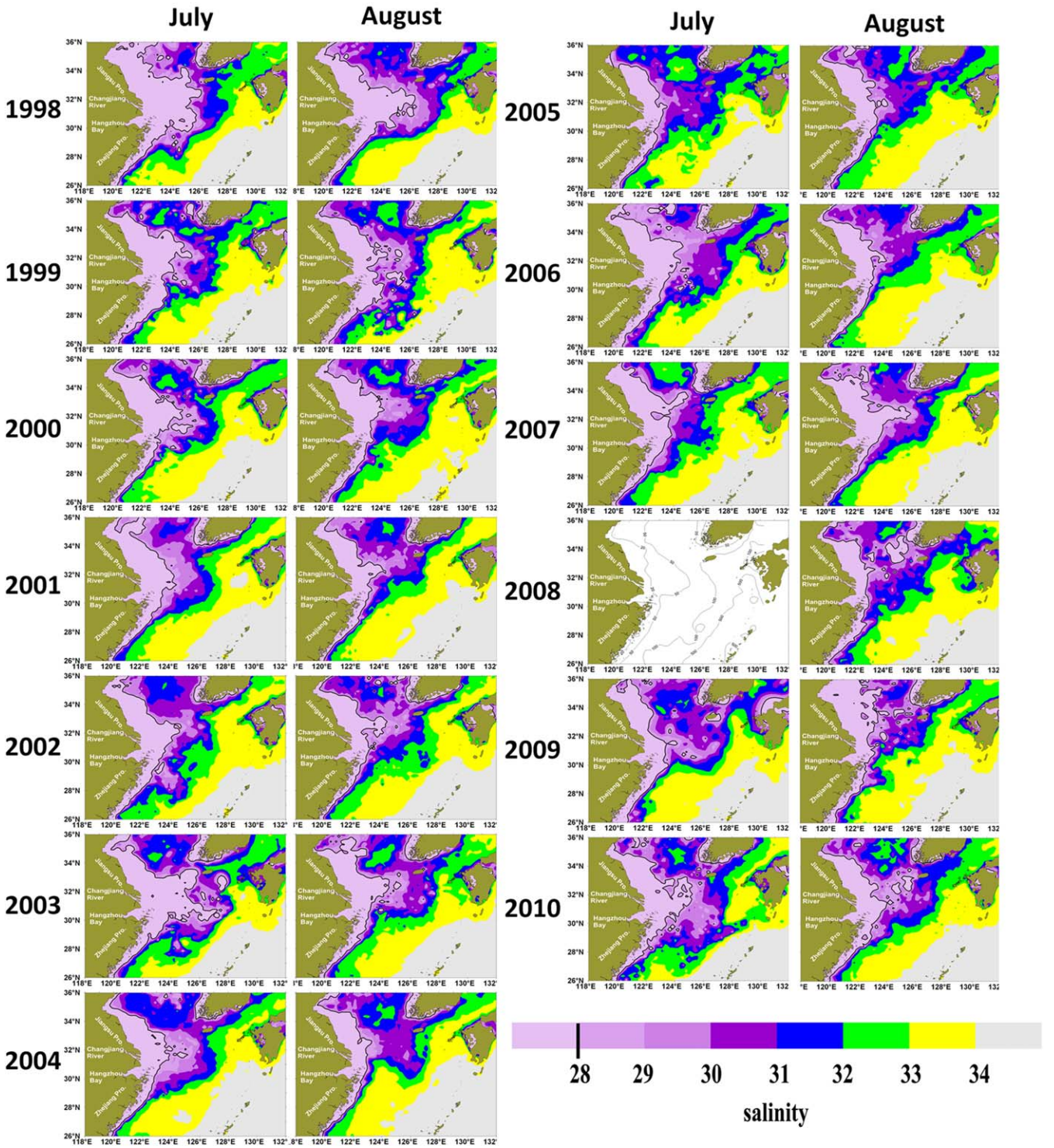

Figure 5. Satellite-derived monthly Changjiang River plume distribution in July and August during 1998–2010. Data are unavailable for July 2008 owing to sensor failure.

Straits both through the Cheju Strait and the south of Cheju Island. Type 1 includes all cases that do not belong to types 2 and 3.

Type 2 plumes extend entirely northeastward with most of the plume water moving northward to the southern Yellow Sea and then being advected eastward through the Cheju Strait with less low-salinity water staying on the middle shelf of the southern ECS. Such cases are generally found in August. During 1998–

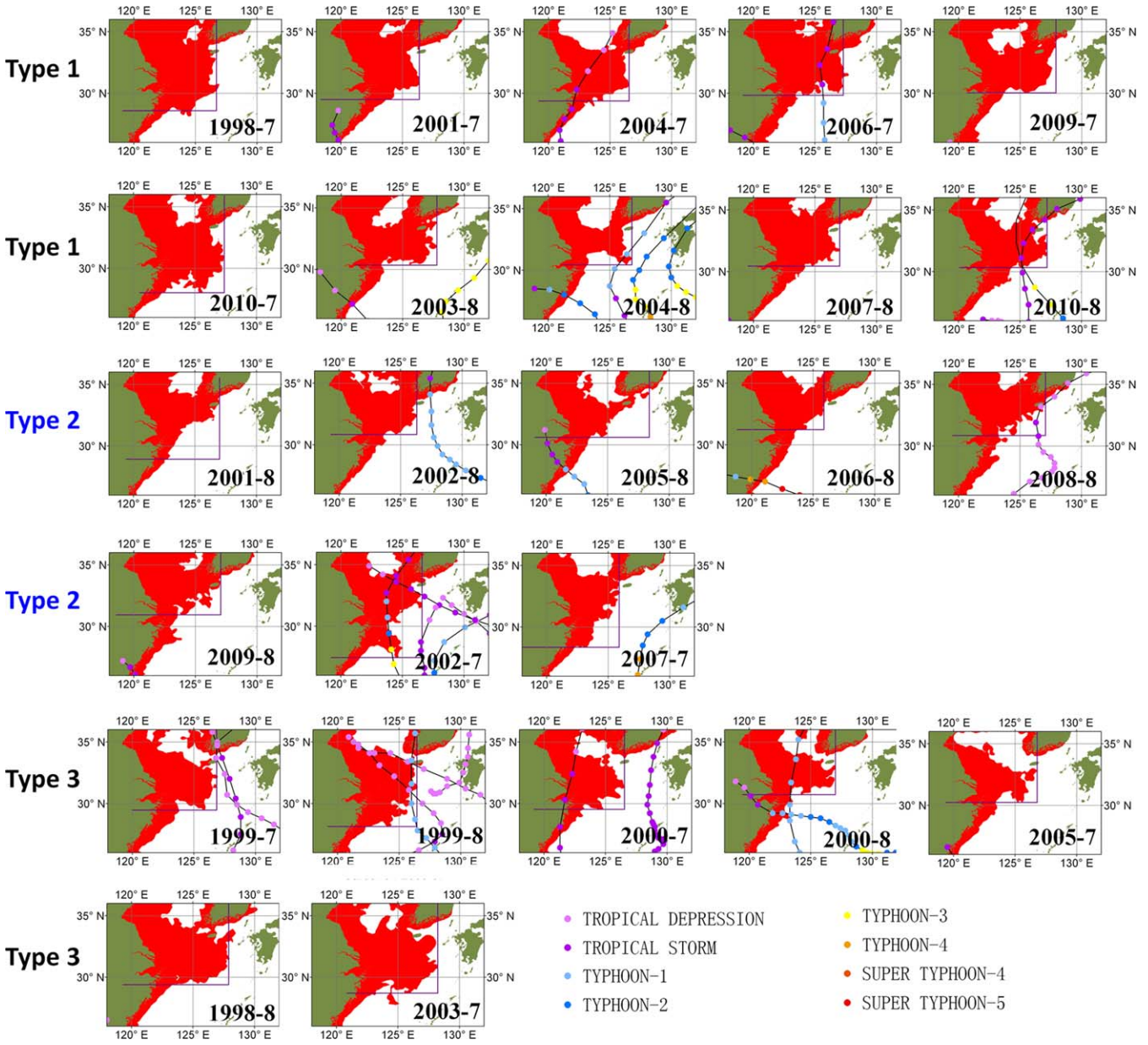

Figure 6. Plume types from the monthly salinity field within the 31 isohaline in July and August over 1998–2010 overlaid with typhoon tracks.

2010, plumes in July 2002 and 2007 and August 2001, 2002, 2005, 2006, 2008, and 2009 belong to this type (Figure 6). Such plumes can also be found in the monthly salinity maps from the KODC in situ data in August 2001 and 2005 (Figure 4), where the low-salinity water masses have a significant northeastward (near the 45° direction) jet shape toward the western channel of the Tsushima-Korea Straits. Overall, the major difference between types 1 and 2 is that type 2 plumes mostly cross the Cheju Strait with only a small fraction staying on the shelf of the ECS, whereas type 1 plumes transport both through the Cheju Strait and the south of Cheju Island.

Type 3 plumes have a significant southeastward tongue in the front, and less plume water enters the Cheju Strait and the Tsushima-Korea Straits. Plumes in July 1999, 2000, and 2005 and August 1999 and 2000 belong to this type. They move more southeastward, in contrast to the northward movement of type 1 and type 2 plumes (Figure 6). In the cases with large plume area, such as in July 2003, July 2010, and August 1998, the plumes show a significant eastward trend and are nearly rectangle in shape, with the eastern boundary of 31 isohalines reaching to 127°–128°E. For plumes in July 2003 and 2010, the southern

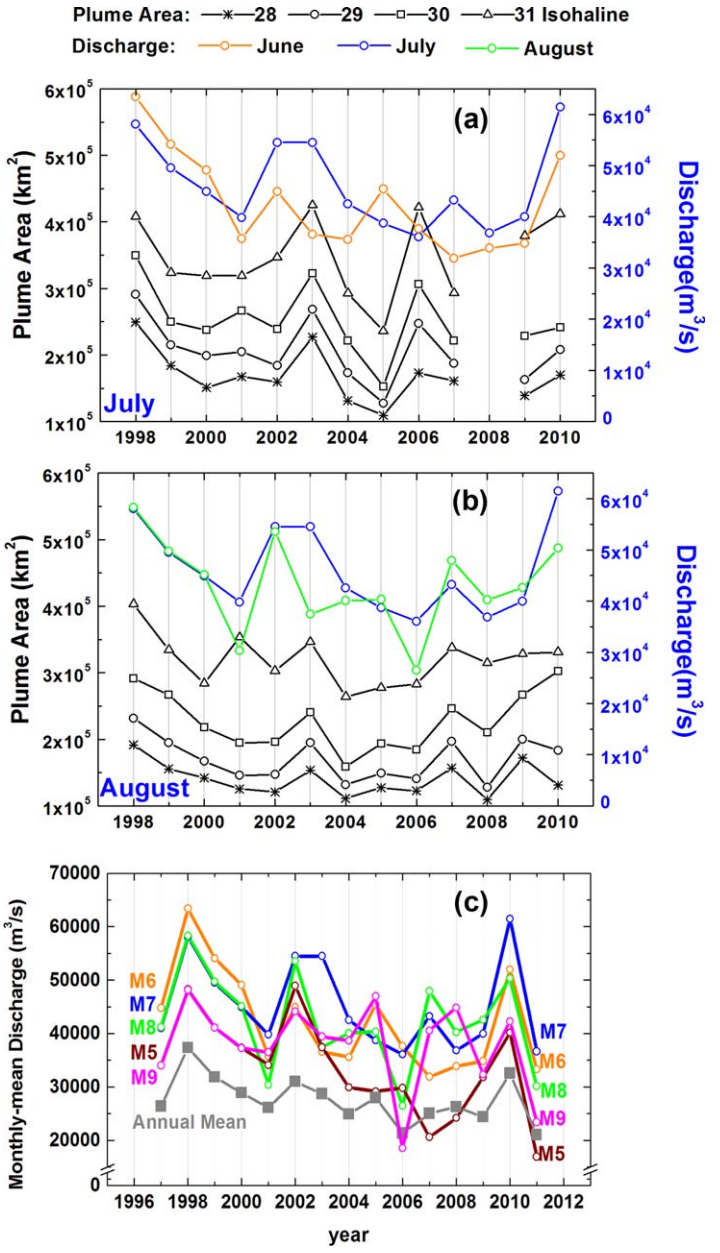

Figure 7. Interannual variation of monthly Changjiang River discharge and plume area, showing the plume area with salinity thresholds of 28, 29, 30, and 31 in (a) July and(b) August compared with the discharge. (c) Changjiang River discharge in May, June, July, August, and September (marked as M5, M6, M7, M8, and M9, respectively) and the annual mean discharge averaged from monthly values (marked as a gray line with square dots).

boundary of 31 isohalines can even reach to 28°N. The case of late August 1998 was discussed in *Lie et al*. [2003], who found an eastward continuation of low-salinity water south of Cheju Island but observed no plume water in the Cheju Strait or in the northwestern area of Cheju Island in August.

4.2. Interannual Variation of Plume Area in Summer

Plume areas in July and August during 1998–2010 were calculated based on the area confined by the individual 28, 29, 30, and 31 isohalines (Figure 7). Overall, the interannual variation of plume areas at each isohaline exhibited an approximately similar trend. Although the areas of the 31 isohaline were significantly larger than those of isohalines of lower salinity values in both of July and August, their fluctuations are similar, except in August 2001. Plume area increased faster than the linear increase of salinity. As the plume extends, freshwater gets mixed with the salty marine water in multiple directions. In addition, the plume weakens as the extension area increases, which might make it more vulnerable to the impact of environmental change.

Generally, the plume area in August was smaller than in July especially for the lower isohalines. In July, the average area of the 31 isohaline was $(34.8 \pm 6.0) \times 10^4$ km^2 during 1998–2010. There were four remarkable peaks in July (1998, 2003, 2006, and 2010), but in July 2005 the plume had a significantly smaller area (Figure 7a). In comparison, the average area of the 31 isohaline in August was only $(32.0 \pm 3.8) \times 10^4$ km^2, with a smaller interannual variation (Figure 7b). However, large plume areas were found in August 1998, 2001, and 2003; from 2007 to 2010, plume areas in August maintain a similar high level.

4.3. Interannual Variation of River Discharge and Wind Field in Summer

The summers of 1998 and 2010 were significant large flood times for the Changjiang River (Figure 7c). During 1998–2002 and 2008–2010, discharges in June, July, and August show similar variational trends, which were also similar to the variation of plume area in July and August. However, monthly discharges were

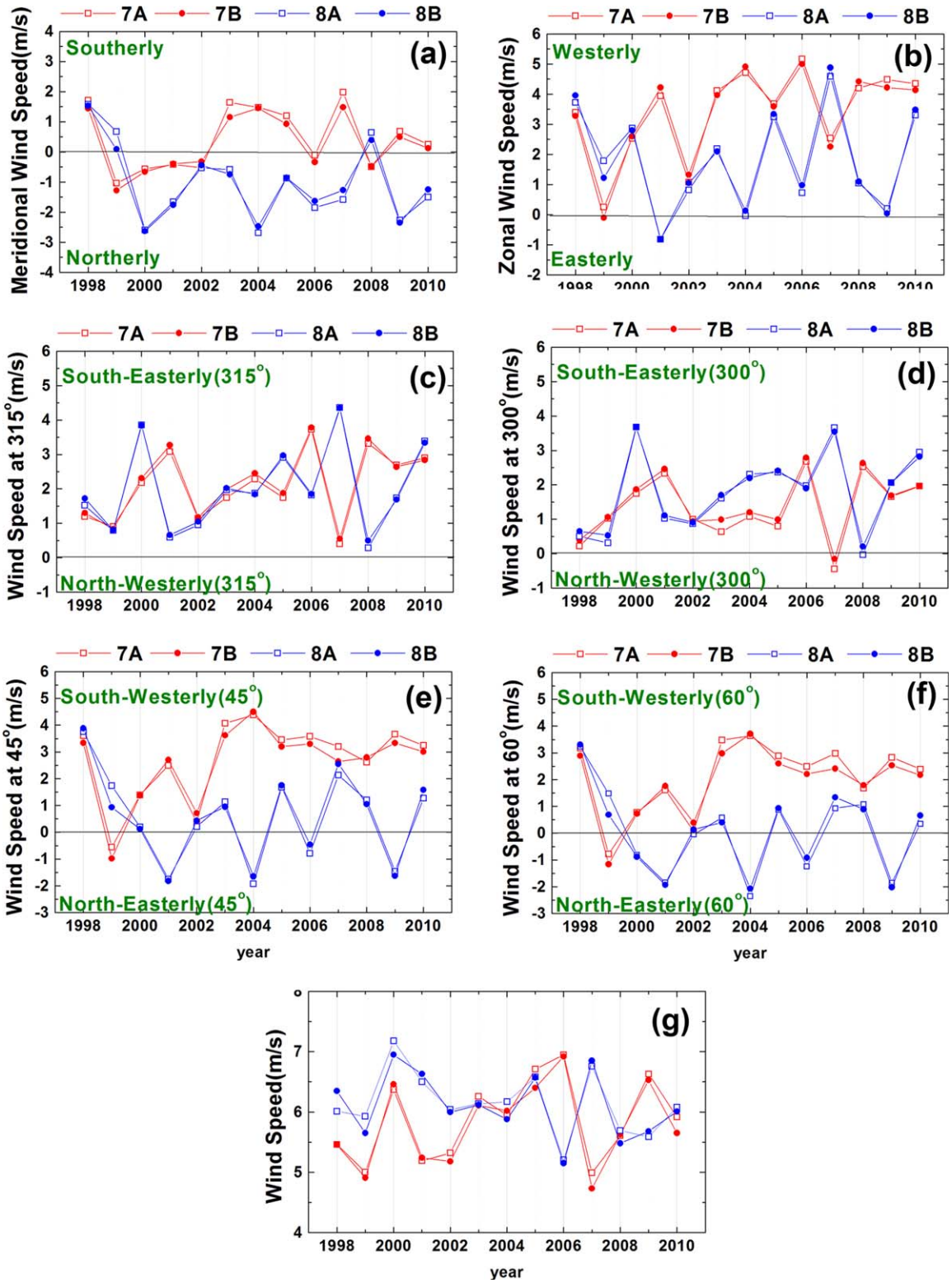

Figure 8. Variation in the monthly wind field for July and August from the CCMP data set during 1998–2010. Values are averaged in two boxes in Figure 1 for comparison (box A: 124°–127°E, 29°–32°N; box B: 124°–126°E, 30°–32°N) and the similarity of the results in these two boxes indicate that the impact of the box size is negligible. (a) Meridional wind speeds, with positive (+) and negative (−) signs denoting southerly and northerly wind components, respectively. (b) Zonal wind speeds, with positive (+) and negative (−) signs denoting westerly and easterly wind components, respectively. (c and d) Wind speeds in the 315° and 300°direction, with positive (+) and negative (−) signs denoting southeasterly and northwesterly wind components, respectively. (e and f) Wind speeds in the 45° and 60° direction, with positive (+) and negative (−) signs denoting southwesterly and northeasterly wind components, respectively. (g) Variation in total wind speeds.

fluctuating during 2003–2007 between the summer months, and their relationships with plume area were complicated, indicating that other factors beyond discharge influence the plume area.

We checked the wind field in the middle of the ECS, where the extension of plume may be vulnerable. The interannual variation of wind speed was significant in summer during 1998–2010 (Figure 8). Both the meridional and zonal wind components were very different in July and August (Figures 8a and 8b). The southerly wind components were dominant in July, and the northerly winds were increasing in August. The westerly wind components were dominant in both July and August, but they were larger in July than in August. The southeasterly wind (300° or 315° wind) was prevailing both in July and August, and there were almost no northwesterly wind components during these two months (Figures 8c and 8d). The southwesterly wind (60° or 45° wind) prevailed in July, except 1999, whereas northeasterly wind was dominant in August 2001, 2004, 2006, and 2009 (Figures 8e and 8f).

5. Discussion

The extension of the Changjiang River plume is complex and may be influenced by river discharge and oceanic environment, such as the wind field, the northward Taiwan Warm Current, the Kuroshio, and tides [e.g., *Chang and Isobe*, 2003; *Lee and Chao*, 2003; *Moon et al*., 2009]. In this study, however, we focus only on discussing the possible influence of river discharge and wind field (including typhoons) changes on the plume extension using the time-series data over 1998–2010, owing to the lack of other time-series hydrological and biogeochemical data. We also discuss a few special cases beyond the general trends in the hope of stimulating further mechanistic studies.

5.1. Effects of the River Discharge and Wind Field on the Plume Area

The plume areas in July generally have a significant relationship to the discharge in July (Figure 9a and Table 1), although the river discharge has a time lag from the hydrological Datong Gauge Station to the river mouth and further across the shelf. However, the plume areas in July do not correlate well with the discharge in June or the cumulative discharge two months before (a value obtained by simply adding together the discharges in May and June) (Figures 9c and 9e). In contrast, the plume areas in August have no significant relation to the discharge in the same month (Figure 9b), but they correlate well with the discharge one month before (July) and the cumulative discharge in June and July (Figures 9d and 9f). Based on the SeaWiFS-derived time-series chlorophyll products over 1998–2007, *Kim et al*. [2009] also found that the Changjiang River discharge in July largely determined the plume area from August to September. The reason for the different plume behaviors in July and August may be that the discharge in July was generally the largest in the year and dominates the plume extension, whereas the discharge in August was weaker and other factors may play a more significant role. Meanwhile, the southwest monsoon prevails in July (Figure 8), and the plume's eastward extension was further enhanced by eastward Ekman transport [*Lie et al*., 2003; *Chang and Isobe*, 2003; *Siswanto et al*., 2008]. However, in August, the southwest monsoon weakens and the frequency of northeast winds increases (Figure 8).

For the effects of wind field on the plume, *Siswanto et al*. [2008] found that the eastward extension of the 32 isohaline of the Changjiang River plume had significant positive correlations with both the meridional wind ($R = 0.47$) and the zonal wind ($R = 0.44$) based on the in situ data from 1950 to 2002, although the area of their study was relatively small (within a small region from 31° to 32°N and from 122.5° to 130°E). However, *Kim et al*. [2009] found that meridional wind had only weak correlations with the area of high satellite-derived chlorophyll *a* (considered as the plume area) in the region of 28°–34°N and 122°–129°E with no time lag from July to September ($R^2 = 0.11$, 0.59, and 0.45, respectively) over the period 2000–2007. As result of a wider coverage of plume extension, especially in the north of the Changjiang Estuary, than that of *Siswanto et al*. [2008] and *Kim et al*. [2009], our plume areas do not show significant relationships with the meridional wind, zonal wind (Figures not showed), or southeasterly wind (Figure 10) in either July or August 1998–2010, indicating the complexity of the plume extension. However, the plume areas in August have positive correlation with the southwesterly wind, whereas no such relationship was found in July (Figure 10), meaning that the plume area in August may be more vulnerable to the southwesterly wind under smaller river discharge conditions. This may partly explain the fact that plume areas in August do not show significant correlation with the discharge in the same month, unlike that in July. It may be argued that the plume extension should be better correlated with the southeasterly wind than with the southwesterly wind according to wind-driven Ekman transport. However, although the southeasterly wind could enhance

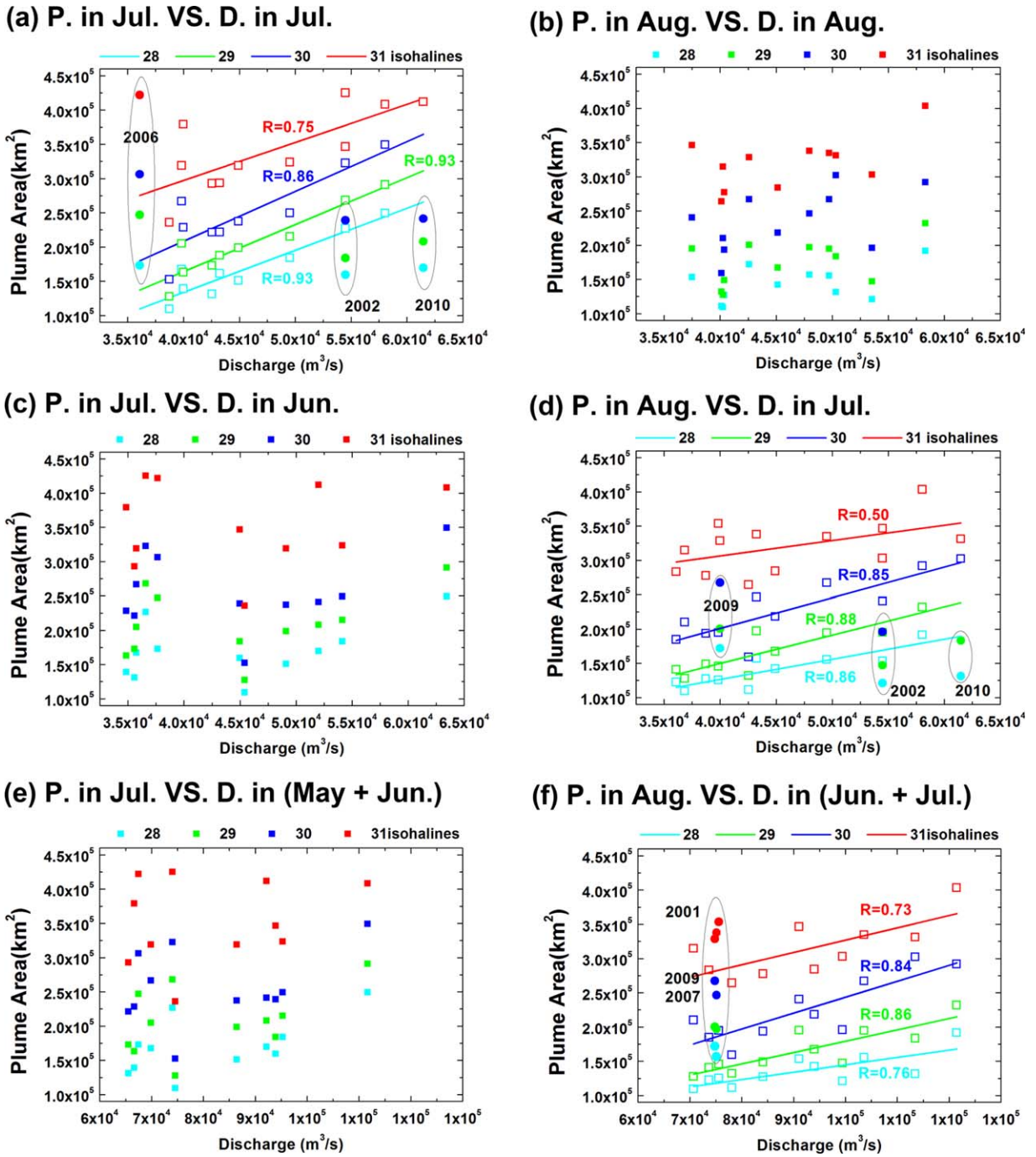

Figure 9. Relationships between the plume area (P) and monthly discharge (D) areas. Figures in the left column and the right column show the plume areas in July and August, respectively. The solid color circles in Figures 9a, 9d, and 9f are the obviously specific cases beyond the generally regressive trend; these are excluded in the linear regression between the discharge and plume area. Regression results are shown in Table 1.

and accelerate the northeastward volume transport of the plume, the plume area may not be significantly increased. In contrast, the southwesterly wind will induce a southeastward extension of the plume in the surface layer, which may cause a wider spread of the plume into the ECS shelf and increase the plume area more significantly than the southeasterly wind. Thus, plume areas are very dynamic and different between July and August, even on shorter time scales [*Lie et al.*, 2003; *Moon et al.*, 2009]. Owing to the complex nature of the dynamic plume movement, more data in vertical profiles are needed to establish the characteristics of volume transportation of freshwater on shorter time scales.

Table 1. Regression Results of Discharge and Plume Area[a]

X Discharge (m^3/s)	Y Plume area (km^2)	A Offset	B Slope	R	SD	N	P
M7	M7-S28	−111119.78	6.127	0.93	17624.13	9	0.0003
	M7-S29	−110660.61	6.869	0.93	20164.22	9	0.0003
	M7-S30	−82328.59	7.271	0.86	32201.10	9	0.0032
	M7-S31	75137.76	5.553	0.75	40934.62	11	0.0073
M7	M8-S28	8802.03	2.944	0.86	13593.27	10	0.0013
	M8-S29	−14850.60	4.119	0.88	17358.22	10	0.0007
	M8-S30	22635.42	4.468	0.85	25212.31	11	0.0009
	M8-S31	216471.45	2.247	0.50	34358.85	13	0.0799
M6+M7	M8-S28	37390.74	1.074	0.76	16535.11	11	0.0072
	M8-S29	13771.22	1.655	0.86	17784.70	11	0.0008
	M8-S30	11196.22	2.323	0.84	26104.41	11	0.0011
	M8-S31	147171.74	1.797	0.73	30158.60	10	0.0167

[a]Note: The linear regression equation is $Y=A+B*X$. In column *X*, M6, M7, and (M6+M7) mean the discharge in June, July, and June plus July, respectively. In column *Y*, M7-S28 means the plume area in the 28 isohaline (S28) in July (M7), and the other codes have similar meanings. R and SD are the regression coefficient and the standard deviation, respectively. N and P are the number of valid samples and the significance of regression, respectively.

5.2. Pathways of Plume Extension in the ECS

From the classification of the three types of Changjiang River plume identified by the 31 isohalines in Figure 6, we can draw a schematic map of the plume pathways (Figure 11). Those pathways have been verified in some cases by using satellite-tracked drifters [*Lie et al*., 2003; *Matsuno et al*., 2006; *Chen et al*., 2008a; *Moon et al*., 2009]. There are generally two pathways by which the low-salinity plume patches are advected to the Tsushima-Korea Straits: 1. through the south of Cheju Island, with the low-salinity water being advected by the Kuroshio Branch Current (also known as the Tsushima Warm Current) [*Lie et al*., 2003], and 2. by the plume extending northward along the China coast first and then turning eastward through the Cheju Strait [*Lie et al*., 2000, 2003; *Chen et al*., 2008a], which was defined as our type 2 plume. *Lie et al*. [2000, 2003] pointed out that the eastward flowing Cheju Warm Current in the Cheju Strait prevents the Korean coastal water from extending southward across the Cheju Strait. Low-salinity water north of Cheju Island clearly shows the Changjiang River plume across the Cheju Strait, although the plume through the Cheju Strait connects with the coastal water of the Korean Peninsula and it is hard to distinguish the two water masses in Figure 5. Similar to the behavior of type 2 plumes, type 1 plumes also cross the Cheju Strait, yet they transport water south of Cheju Island at the same time. Actually, type 2 and type 3 plumes can also be regarded as special cases of the traditional northeastward type 1 plume. In this paper, we will focus on the discussion of these special cases, as these have seldom be studied in previous investigations.

Most type 2 plumes are found in August and exhibit less eastward movement south of Cheju Island, under the condition of smaller wind components in the 45° direction and relatively small discharge in August. From a climatological model study on a monthly scale, *Chang and Isobe* [2003] found that the intrusion of less saline water into the Cheju Strait was more noticeable in August than in July. Plumes in July 2002 and 2007 also belong to the type 2 plume with a smaller plume area but with a large discharge in July. The different situations in these two months need further examination regarding the depth of the freshwater column and the wind field changes on time scales shorter than the monthly average. In general, type 2 plumes have a small area because the majority of freshwater transports through the Cheju Strait and most of the ECS outer shelf are covered by salty water (Figure 6 and Table 2).

In stark contrast to the scenario for type 1 and type 2 plume shapes, type 3 plumes have nearly no plume water entering the Cheju Strait. Compared with type 2 plumes, type 3 plumes move more southeastwardly once they get south of Cheju Island. The eastern boundaries of the 31 isohaline of type 3 plumes (July 1999, 2000, and 2005 and August 1999 and 2000) were all restricted to the west of 127°E, the cause of which cannot be discerned from the monthly wind field. The passage of typhoons (and/or tropical storms) and continuously strong cyclonic wind may be a main factor restricting the plume's eastward transportation and triggering its southward movement. In August 1999, there were four typhoons across the ECS and the plume's southern boundary can even reach to 28°N. Note that although the presence of typhoons may partially explain the extension of type 3 plumes, this is not a necessary condition for plume type classification; the changes of plume shapes depend on the typhoon's moving track and the magnitude of the changing wind field. A similar southward movement of plume fronts belonging to type 1 caused by northward-

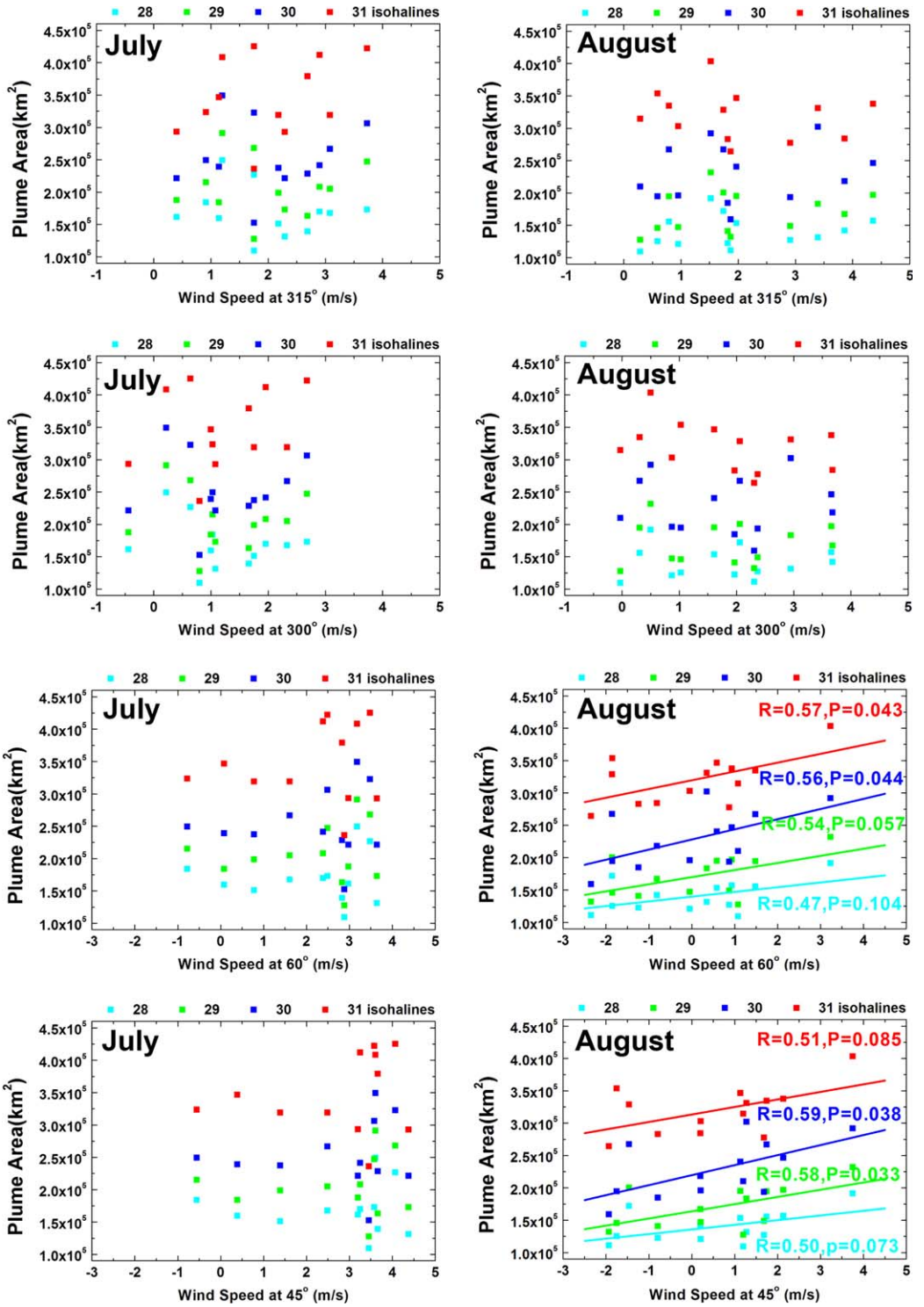

Figure 10. Relationships between the plume area and wind speed components in region A (124°–127°E, 29°–32°N) (Figure 1). For the meaning of wind components refer to the caption of Figure 8.

moving typhoons was found in July 2006 and August 2004. Although four typhoons passed northeastward in August 2004, none entered the middle shelf of the northern ECS. One might argue that the passage of typhoons brings a significant amount of rain and lowers the salinity of seawater; however, typhoon-induced

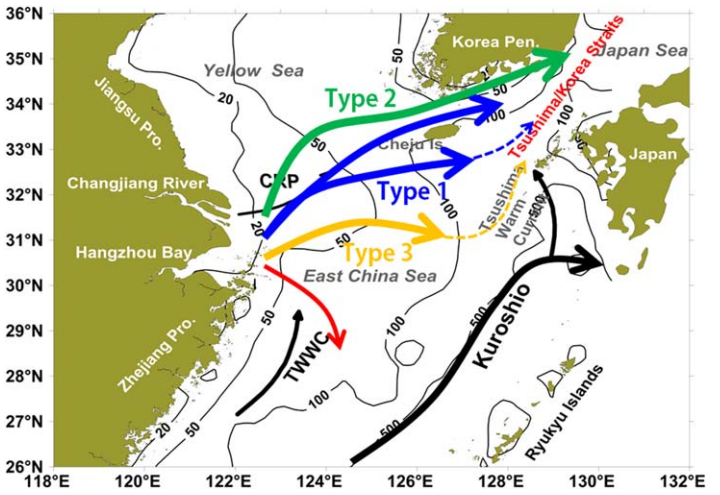

Figure 11. Schematic pathways (colored arrows) of the three types of Changjiang River plume identified from the 31 isohalines. The dashed arrows in blue and yellow signify plume water higher than the 31 salinity unit would have advected by the Tsushima Warm Current (Kuroshio Branch Current) to the Tsushima-Korea Straits. The red arrow shows the occasional movement triggered by typhoons.

rains would not have high CDOM concentration; they should decrease the a_{CDOM} through dilution and correspondingly increase the CDOM-based salinity. Therefore, the satellite-derived low-salinity water in the ECS reflects the extension of the river plume.

Another kind of low-salinity water mass penetrating the shelf was also found south of the Changjiang Estuary (near 28.5°–30°N; plumes in July 2002 and July 2007 in Figures 5 and 6 and August 2009 in Figure 5). The mechanism of such cross-shelf penetrating fronts was complex and depends on interactions with the wind field and the Taiwan Warm Current [*Yuan et al.*, 2005; *He et al.*, 2010]. Here we speculate that the episodic typhoon events and corresponding wind field changes, which are seldom discussed in the literature, may significantly affect such extension of the plume. A good example is that the locations of multiple low-salinity fronts in July 2002 are consistent with typhoon tracks. In contrast to the general northeastward plume, these typhoon-triggered low-salinity water fronts that occasionally appear to the south of the ECS might have a noticeable effect on plume-related processing and materials transportation, and such phenomena cannot always be captured by a field campaign.

Generally, compared with the normally northeastward movement of type 1 plumes, type 2 and type 3 plumes have relative small areas as the extensions are confined, although special cases exist (Table 2). A detailed mechanism analysis still needs more data and would need to be performed in conjunction with modeling studies. Although our classification of plume types is now quite qualitative, and the instant extension of the plume is very complex and may shift in any way on smaller scales, we have provided a generally new view on the plume extension on the monthly scale and its linkage to the river discharge and wind field.

Table 2. Plume Area of the 31 Isohaline, Monthly Mean Discharge, Wind Speed in the 45° Direction (Southwesterly Wind), and Plume Type in July and August During 1998–2010

	July				August			
Year	Plume Area (km^2)	Discharge (m^3/s)	Wind[a] (m/s)	Plume Type	Plume Area (km^2)	Discharge (m^3/s)	Wind[a] (m/s)	Plume Type
1998	408218.5	58042.0	3.61	1	403390.1	58300.1	3.75	3
1999	323748.0	49513.6	−0.56	3	334684.2	49733.8	1.74	3
2000	318991.0	44921.4	1.39	3	284186.2	45121.2	0.2	3
2001	318991.0	39845.5	2.49	1	353604.4	30378.0	−1.75	2
2002	346503.1	54489.9	0.39	2	302982.4	53546.7	0.21	2
2003	425179.5	54492.3	4.07	3	346465.8	37482.2	1.13	1
2004	292783.7	42546.5	4.38	1	264248.2	40098.6	−1.93	1
2005	235935.7	38729.8	3.45	3	277592.1	40343.6	1.68	2
2006	422047.8	36074.9	3.58	1	283111.8	26457.4	−0.79	2
2007	293276.6	43248.6	3.2	2	337723.7	47948.7	2.13	1
2008	/[b]	36839.1	2.62	/	314790.5	40256.2	1.2	2
2009	379111.2	39991.8	3.66	1	328582.7	42592.5	−1.46	2
2010	412045.0	61471.6	3.25	1	331238.8	50311.8	1.27	1

[a]Wind speeds in the 45° direction, with positive (+) and negative (−) signs denoting southwesterly and northeasterly wind components, respectively.
[b]Satellite data are unavailable for July 2008 owing to sensor failure.

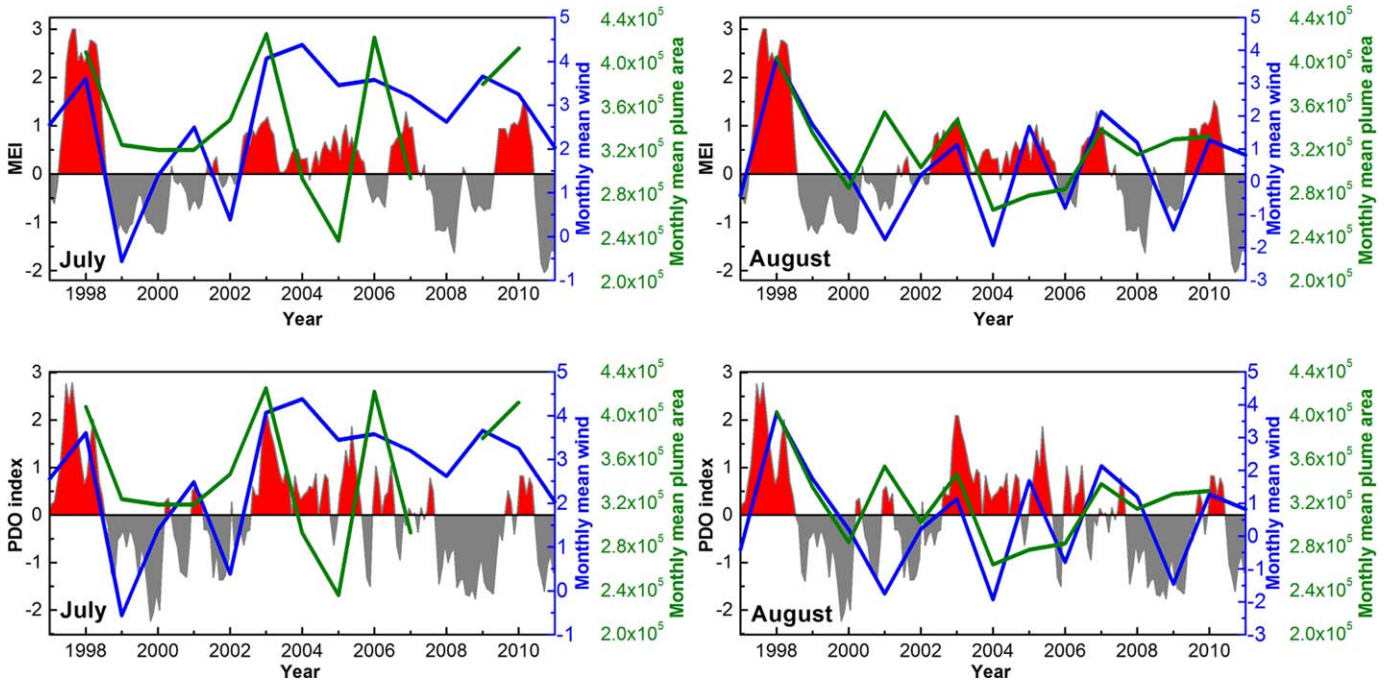

Figure 12. Comparisons of the interannual variations among monthly mean wind speed in the 45° direction (southwesterly wind) and the MEI and PDO indices in July and August.

5.3. Natural Variation and Anthropogenic Effects

The interannual variation of the Changjiang River plume can be regulated by natural variation and anthropogenic effects, since both can alter the river discharge. *Siswanto et al.* [2008] reported that the summer surface salinity in the northern ECS exhibited an overall decreasing trend from 1951 to 2001 with the increase of Changjiang River discharge and precipitation anomaly over the Changjiang River valley. However, we do not find a general temporal trend in plume area change over the period of 1998–2010. Although a period of 13 years (1998–2010) is too short to evaluate the effects of climate change on the long-term trends of the Changjiang River plume area, we still can examine the possible correlation of their interannual variations. It was widely reported that there are good correlations between the Changjiang River discharge and the ENSO and PDO indices, with large discharges generally corresponding to warm phases of ENSO and PDO or vice versa [*Jiang et al.*, 2006; *Zhang et al.*, 2007; *Siswanto et al.*, 2008; *He et al.*, 2013a]. Since the plume areas in both July and August have a significant correlation with the discharge in July (Figure 9a), they covary with the natural climate variation, as shown in Figure 12. This means that changes in climate and the corresponding marine environment leave significant footprints on the plume area variation, but further insights need longer time-series data from stable monitoring systems, e.g., satellite observation and time-series stations.

During the past decade, the impacts of the construction of the Three Gorges Dam on the physical and biogeochemical environments of the ECS shelf and its surrounding oceans have received extensive attention. Many researchers noted that sediment transportation had decreased significantly from the Changjiang River to the ECS because of the Three Gorges Dam [e.g., *Xu et al.*, 2006; *Chu et al.*, 2009; *Gao and Wang*, 2008]. However, the river discharge and sediment flux do not necessarily covary [*Gao and Wang*, 2008]. Unlike the particles that were retained by the dams, the effect of the Three Gorges Dam on the discharge was less obvious, only acting to adjustments of the variation in flow between months. We can see that the monthly discharges of June, July, and August in Figure 7c show remarkably different interannual variation over 2003–2007.

Owing to limited time-series data of other parameters, it is still hard to distinguish natural variation and that caused by human activity over the short period of 13 years (1998–2010). Instead, we used two special years, 2003 and 2006, to further discuss this issue as they were often used to illustrate the combined effects of the Three Gorges Dam and natural variation on the reduction of the discharge and plume and the impacts on biogeochemistry [e.g., *Gong et al.*, 2006; *Yuan et al.*, 2007; *Dai et al.*, 2008; *Tseng et al.*, 2011].

In June 2003, the Three Gorges Dam was first impounded, raising the water level to 135 m. Because of water retention, the discharges in June and August were kept to a low level (~37,000 m^3/s). In contrast, the discharge in the peak rainy month of July was at a high level (~54,500 m^3/s). *Gong et al*. [2006] concluded that primary production decreased after the filling of the Three Gorges Dam in June 2003 based on data from four cruises; however, based on satellite chlorophyll *a* data, *Yuan et al*. [2007] pointed out that it was a result of a sampling bias within this highly variable system. Based on the satellite-derived salinity data, we found that the satellite-derived plume area in July 2003 (31 isohaline) extended to 128.2°E and 28.7°N, which was substantially higher than the mean plume over 1998–2010. This large plume area in July 2003 was consistent with the high chlorophyll *a* in the plume found by *Kim et al*. [2009]. However, in August 2003, the plume moved northward, with the southern boundary of the 31 isohaline retreating to 30.3°N, but its eastern boundary still reached 127.8°E. Using the SeaWiFS-derived time-series chlorophyll *a* data, *Kim et al*. [2009] also found that the area of the offshore Changjiang River plume did not seem to be critically reduced after the first impounding of the Three Gorges Dam in the summer of 2003. *Yuan et al*.'s [2007] analysis also indicated that there was no apparent decline in the chlorophyll *a* level that can be attributed to the damming in 2003. Similarly, *Yamaguchi et al*. [2012] found that the mean satellite-derived chlorophyll *a* concentration in the offshore of the Changjiang River mouth to around Cheju Island during the summer of 2003 were in the middle range of values found between 1997 and 2006.

Similarly, year 2006 was the worst drought year in the past 50 years, coinciding with the rising of the water level in the Three Gorges Dam from 135 to 156 m [*Dai et al*., 2008; *Chu et al*., 2009]. However, the plume area in July 2006 was still one of the largest between 1998 and 2010. Correspondingly, the phytoplankton bloom intensity was also high in the summer of 2006, beyond the general positive correlation between bloom intensity and river discharge, and the position of the bloom was more northerly than in other years [*He et al*., 2013a]. Using three-dimensional modeling in August 2002 and 2006, *Moon et al*. [2009] found that the low river discharge as a flood control scenario had little influence on the spatial behavior of the Changjiang River plume around Cheju Island although the discharge contributes to the amount of freshwater around Cheju Island.

Therefore, it appears that the influence of the Three Gorges Dam on the plume area in summer is limited over the period of 1998–2010, and the interannual variation of the plume area extension was probably regulated more by natural variation than by anthropogenic effects. More data are still needed to get further insights.

6. Conclusions and Implications

In this study, based on abundant independent in situ data, we further improved *Bai et al*.'s [2013] satellite-derived salinity algorithm in the ECS to make it more specific and accurate for summer. With the time-series satellite-derived salinity data, we presented and examined the interannual variation of the Changjiang River plume extension in summer months during 1998–2010. Three types of plume shapes were identified. Besides the common northeastward extending plumes in summer, two additional types of plume extensions exist, though they are seldom recorded by previous field measurements. In one case, most of the freshwater was transported through the Cheju Strait with only a small fraction staying on the ECS outer shelf; in the other case, the plume moved southeastwardly with less plume water crossing the Cheju Strait. More importantly, we quantitatively clarified the relationships between plume areas and river discharges. During 1998–2010, plume areas in July were generally larger than in August of the same year. With larger river discharge and a favorable southwesterly monsoon, plume areas in July were positively correlated with river discharge in the same month. In contrast, the plume areas in August were generally positively correlated with the discharge in July rather than that in August. In addition, the plume areas in August also had a positive relationship with the southwesterly wind speed, indicating that the plume extension in August was more vulnerable to southwesterly wind under the relatively low discharge than that in July. Although the instant extension of the plume is very complex and may shift in any way on small scales, our classification of the types of plume shapes should be helpful for providing a general new view on plume extension on a monthly scale and its linkage to river discharge and the wind field. In addition, our results indicate that one should be cautious in judging the change of plume area and relative biogeochemical processes without first forming a complete view of plume extension.

Human activities have inevitable effects on large river-dominated marginal seas. In addition to the adjustment of water discharge from dams along the Changjiang River, China's ongoing South-to-North Water

Transfer Project for supplying water to the semi-arid regions of northern China will remove ~5% of the Changjiang water, leading to a 3%–5% sediment loss [*Yang et al*., 2002]. These construction projects would lengthen the flushing time for river water in wet seasons but shorten it in dry seasons [*Gao and Wang*, 2008; *Chen et al*., 2008b]. If the movement of the plume becomes relatively slow in summer, then fewer nutrients may be supplied by upwelling from bottom water generated by the horizontal divergence of the Changjiang River plume [*Chen*, 2000; *Isobe and Matsuno*, 2008]. Correspondingly, primary production, fisheries landings, and biogeochemical processes could all be affected. Meanwhile, unlike the particles blocked by the dams, terrestrial dissolved material (e.g., dissolved organic carbon (DOC)) transported by the plume can move greater distances, and the influence of plume variation on DOC transportation should be noted, as DOC is a good food source for bacteria and an important component of the carbon cycle in marginal seas [*Jiao et al*., 2007]. Therefore, accumulating additional time-series satellite-derived plume extension data would be very helpful for plume system studies and reveal the combined effect of natural change and human activities. In addition to monthly maps, refined insights on the behaviors of the Changjiang River plume and its mechanisms could also be provided by the daily satellite-derived salinities, and even from hourly measurements from geostationary satellites ocean color data (e.g., from the Geostationary Ocean Color Imager launched in 2010, which record eight images per day with 500 m spatial resolution) [*He et al*., 2013b].

Acknowledgments

This study was supported by the Public Science and Technology Research Fund Projects for Ocean Research (grant 200905012), the National Basic Research Program ("973" Program) of China (grant 2009CB421202), the National Natural Science Foundation of China (grants 41322039, 41271378, and 41321004), and the National Key Technology Support Program of China (grants 2013BAD13B01 and 2012BAH32B01), and the "Global Change and Air–Sea Interaction" project of China (grant GASI-03-03-01-01). We thank NASA for providing the SeaWiFS satellite data; NODC, KODC, and JMA for providing the salinity data; and CMWR, JTWX and PO.DAAC for providing Changjiang River discharge, typhoon track, and wind field data, respectively. The Associate Editor and three anonymous reviewers have provided many constructive suggestions that helped to significantly improve the manuscript.

References

Ahn, Y. H., P. Shanmugam, J. E. Moon, and J. H. Ryu (2008), Satellite remote sensing of a low-salinity water plume in the East China Sea, *Ann. Geophys.*, *26*, 2019–2035.

Atlas, R., J. Ardizzone, and R.N. Hoffman (2008), Application of satellite surface wind data to ocean wind analysis, *Proc. SPIE*, *7087*, 70870B-70870B-7.

Atlas, R., R. N. Hoffman, J. Ardizzone, S. M. Leidner, J. C. Jusem, D. K. Smith, and D. Gombos (2011), A cross-calibrated, multiplatform ocean surface wind velocity product for meteorological and oceanographic applications, *Bull. Am. Meteorol. Soc.*, *92*(2), 157–174.

Bai, Y., D. Pan, W.-J. Cai, X. He, D. Wang, B. Tao, and Q. Zhu (2013), Remote sensing of salinity from satellite-derived CDOM in the Changjiang River dominated East China Sea, *J. Geophys. Res. Oceans*, *118*, 227–243, doi:10.1029/2012JC008467.

Bailey, S. W., and P. J. Werdell (2006), A multi-sensor approach for the on-orbit validation of ocean color satellite data products, *Remote Sens. Environ.*, *102*, 12−23.

Carder, K. L., F. R. Chen, Z. Lee, S. K. Hawes, and J. P. Cannizzaro (2003), MODIS ocean science team algorithm theoretical basis document, ATBD 19, 67 pp., NASA, Washington, D. C. [Available at http://modis.gsfc.nasa.gov/data/atbd/atbd_mod19.pdf.]

Chang, P. H., and A. Isobe (2003), A numerical study on the Changjiang diluted water in the Yellow and East China Sea, *J. Geophys. Res.*, *108*(C9), 3299, doi:10.1029/2002JC001749.

Chen, C., R. C. Beardsley, R. Limeburner, and K. Kim (1994), Comparison of winter and summer hydrographic observations in the Yellow and East China Sea and adjacent Kuroshio during 1986, *Cont. Shelf Res.*, *14*, 909–929.

Chen, C., et al. (2008a), Physical mechanisms for the offshore detachment of the Changjiang Diluted Water in the East China Sea, *J. Geophys. Res.*, *113*, C02002, doi:10.1029/2006JC003994.

Chen, C.-C., F.-K. Shiah, K.-P. Chiang, G.-C. Gong, and W. M. Kemp (2009), Effects of the Changjiang (Yangtze) River discharge on planktonic community respiration in the East China Sea, *J. Geophys. Res.*, *114*, C03005, doi:10.1029/2008JC004891.

Chen, C. T. A. (2000), The Three Gorges Dam: Reducing the upwelling and thus productivity in the East China Sea, *Geophys. Res. Lett.*, *27*(3), 381–383, doi:10.1029/1999GL002373.

Chen, C. T. A. (2008), Chemical and physical fronts in the Bohai, Yellow and East China seas, *J. Mar. Syst.*, *78*, 394–410.

Chen, C. T. A. (2009), Distributions of nutrients in the East China Sea and the South China Sea connection, *J. Oceanogr.*, *64*(5), 737–751.

Chen, C. T. A., W. D. Zhai, and M. H. Dai (2008b), Riverine input and air-sea CO_2 exchanges near the Changjiang (Yangtze River) Estuary: Status quo and implication on possible future changes in metabolic status, *Cont. Shelf Res.*, *28*, 1476–1482.

Chu, Z. X., S. K. Zhai, X. X. Lu, J. P. Liu, J. X. Xu, and K. H. Xu (2009), A quantitative assessment of human impacts on decrease in sediment flux from major Chinese rivers entering the western Pacific Ocean, *Geophys. Res. Lett.*, *36*, L19603, doi:10.1029/2009GL039513.

Dagg, M., R. Benner, S. Lohrenz, and D. Lawrance (2004), Transformation of dissolved and particulate materials on continental shelves influenced by large rivers: Plume processes, *Cont. Shelf Res.*, *24*, 833–858.

Dai, Z., J. Du, J. Li, W. Li, and J. Chen (2008), Runoff characteristics of the Changjiang River during 2006: Effect of extreme drought and the impounding of the Three Gorges Dam, *Geophys. Res. Lett.*, *35*, L07406, doi:10.1029/2008GL033456.

Gao, S., and Y. P. Wang (2008), Changes in material fluxes from the Changjiang River and their implications on the adjoining continental shelf ecosystem, *Cont. Shelf Res.*, *28*, 1490–1500.

Gong, G.-C., J. Chang, K.-P. Chiang, T.-M. Hsiung, C.-C. Hung, S.-W. Duan, and L. A. Codispoti (2006), Reduction of primary production and changing of nutrient ratio in the East China Sea: Effect of the Three Gorges Dam?, *Geophys. Res. Lett.*, *33*, L07610, doi:10.1029/2006GL025800.

He, L., Y. Li, H. Zhou, D. Yuan (2010), Variability of cross-shelf penetrating fronts in the East China Sea, *Deep Sea Res., Part II*, *57*, 1820–1826.

He, X., Y. Bai, D. Pan, J. Tang, and D. Wang (2012), Atmospheric correction of satellite ocean color imagery using the ultraviolet wavelength for highly turbid waters, *Opt. Express*, *20*(18), 20,754–20,770.

He, X., Y. Bai, D. Pan, C.-T. A. Chen, Q. Chen, D. Wang, and F. Gong (2013a). Satellite views of seasonal and inter-annual variability of phytoplankton blooms in the eastern China seas over the past 14 yr (1998–2011), *Biogeosciences*, *10*, 4721–4739, doi:10.5194/bg-10-4721-2013.

He, X., Y. Bai, D. Pan, N. Huang, X. Dong, J. Chen, C.-T. A. Chen, and Q. Cui (2013b), Using geostationary satellite ocean color data to map the diurnal dynamics of suspended particulate matter in coastal waters, *Remote Sens. Environ.*, *133*, 225–239.

Isobe, A., and T. Matsuno (2008), Long-distance nutrient-transport process in the Changjiang river plume on the East China Sea shelf in summer, *J. Geophys. Res.*, *113*, C04006, doi:10.1029/2007JC004248.

Jiang, T., Q. Zhang, D. M. Zhu, and Y. J. Wu (2006), Yangtze floods and droughts (China) and teleconnections with ENSO activities (1470–2003), *Quat. Int.*, *144*, 29–37.

Jiao, N. Z., et al. (2007), Ecological anomalies in the East China Sea: Impacts of the Three Gorges Dam?, *Water Res.*, *41*, 1287–1293.

Kim, H. C., et al. (2009), Distribution of Changjiang diluted water detected by satellite chlorophyll-a and its inter-annual variation during 1998–2007, *J. Oceanogr.*, *65*, 129–135.

Lee, H.-J., and S.-Y. Chao (2003), A climatological description of circulation in and around the East China Sea, *Deep Sea Res., Part II*, *50*, 1065–1084.

Lie, H.-J., C.-H. Cho, J.-H. Lee, S. Lee, and T. Yuxiang (2000), Seasonal variation of the Cheju Warm Current in the northern East China Sea, *J. Oceanogr.*, *56*, 197–211.

Lie, H. J., C. H. Cho, J. H. Lee, and S. Lee (2003), Structure and eastward extension of the Changjiang River plume in the East China Sea, *J. Geophys. Res.*, *108*(C3), 3077, doi:10.1029/2001JC001194.

Liu, K.-K., T.-H. Peng, P.-T. Shaw, and F. K. Shiah (2003), Circulation and biogeochemical processes in the East China Sea and the vicinity of Taiwan: An overview and a brief synthesis, *Deep Sea Res., Part II*, *50*(6-7), 1055–1064.

Liu, Z. L., and J. P. Gan (2012), Variability of the Kuroshio in the East China Sea derived from satellite altimetry data, *Deep Sea Res., Part I*, *59*, 25–36.

Matsuno, T., J.-S. Lee, M. Shimizu, S.-H. Kim, and I.-C. Pang (2006), Measurements of the turbulent energy dissipation rate ε and an evaluation of the dispersion process of the Changjiang Diluted Water in the East China Sea, *J. Geophys. Res.*, *111*, C11S09, doi:10.1029/2005JC003196.

Moon, J. H., I. C. Pang, and J. H. Yoon (2009), Response of the Changjiang diluted water around Jeju Island to external forcings: A modeling study of 2002 and 2006, *Cont. Shelf Res.*, *29*, 1549–1564. doi:10.1016/j.csr.2009.04.007.

Sasaki, H., E. Siswanto, K. Nishiuchi, K. Tanaka, T. Hasegawa, and J. Ishizaka (2008), Mapping the low salinity Changjiang Diluted Water using satellite-retrieved colored dissolved organic matter (CDOM) in the East China Sea during high river flow season, *Geophys. Res. Lett.*, *35*, L04604, doi:10.1029/2007GL032637.

Siswanto, E., H. Nakata, Y. Matsuoka, K. Tanaka, Y. Kiyomoto, K. Okamura, J. Zhu, and J. Ishizaka (2008), The long-term freshening and nutrient increases in summer surface water in the northern East China Sea in relation to Changjiang discharge variation, *J. Geophys. Res.*, *113*, C10030, doi:10.1029/2008JC004812.

Su, J. (1998), Circulation dynamics of the China Seas north of 18°N, in *The Sea*, vol. 11, edited by A. R. Robinson and K. H. Brink, pp. 483–505, John Wiley, N. Y.

Tseng, C.-M., K. K. Liu, G. C. Gong, P. Y. Shen, and W. J. Cai (2011), CO2 uptake in the East China Sea relying on Changjiang runoff is prone to change, *Geophys. Res. Lett.*, *38*, L24609, doi:10.1029/2011GL049774.

Xu, K., J. D. Milliman, Z. Yang, and H. Wang (2006), Yangtze sediment decline partly from Three Gorges Dam, *Eos Trans. AGU*, *87*(19), 185–190, doi:10.1029/2006EO190001.

Yamaguchi, H., H.-C. Kim, Y.B. Son, S. W. Kim, K. Okamura, Y. Kiyomoto, J. Ishizaka (2012), Seasonal and summer internannual variations of SeaWiFS Chlorophyll a in the Yellow Sea and East China Sea, *Prog. Oceanogr.*, *105*, 22–29, doi:10.1016/j.pocean.2012.04.004.

Yang, S., Q. Zhao, and I. Belkin (2002), Temporal variation in the sediment load of the Yangtze River and the influences of human activities, *J. Hydrol.*, *263*, 56–71.

Yuan, D., F. Qiao, and J. Su (2005), Cross-shelf penetrating fronts off the southeast coast of China observed by MODIS, *Geophys. Res. Lett.*, *32*, L19603, doi:10.1029/2005GL023815.

Yuan, D., J. Zhu, C. Li, and D. Hu (2008), A cross-shelf circulation in the Yellow and East China Seas indicated by MODIS satellite observations, *J. Mar. Syst.*, *70*, 134–149.

Yuan, J., L. Hayden, and M. Dagg (2007), Comment on "Reduction of primary production and changing of nutrient ratio in the East China Sea: Effect of the Three Gorges Dam?" by Gwo-Ching Gong et al., *Geophys. Res. Lett.*, *34*, L14609, doi:10.1029/2006GL029036.

Zhang, Q., C.-Y. Yu, T. Jiang, and Y. J. Wu (2007), Possible influences of ENSO on annual maximum streamflow of the Yangtze River, China, *J. Hydrol.*, *333*, 265–274.

Zhu, W., Q. Yu, Y. Q. Tian, R. F. Chen, and G. B. Gardner (2011), Estimation of chromophoric dissolved organic matter in the Mississippi and Atchafalaya river plume regions using above-surface hyperspectral remote sensing, *J. Geophys. Res.*, *116*, C02011, doi:10.1029/2010JC006523.